Chapter 5

Low-Temperature Solution-Processable Functional Oxide Materials for Printed Electronics

Phan Trong Tue

Additional information is available at the end of the chapter

http://dx.doi.org/10.5772/intechopen.75610

Abstract

Over a decade since the first printed oxide transistor has been reported, printed oxide electronics is now becoming emerging technologies for realization of flexible, large-scale, low-cost electronic devices and systems. This chapter summarizes recent progress in the development of low-temperature solution-processable functional oxide materials and devices, and it also addresses critical challenges for the fundamental understanding and practical implementation of complex oxides in devices. The first part of this chapter gives an overview of the development of functional oxide inks such as semiconductors, conductors, and dielectrics. The second part discusses high-resolution printing technologies and some applications of printed electronics to exemplify their potential.

Keywords: oxide materials, thin-film transistors, oxide semiconductors, oxide dielectrics, transparent conducting oxides, solution process, low-temperature process, printed electronics

1. General introduction

Oxide materials have become high-tech functional materials beyond their traditional role as dielectrics. They show a rich variety of complex emergent behaviors, such as memristive effect [1], catalytic activity [2], and complex multiferroic effects [3]. The discovery of new metal oxides with interesting and useful properties continues to drive much research in chemistry, physics, and materials science. The physicochemical properties of oxides can be tuned through variation of factors such as composition, temperature, pressure, strain, external fields, defects, film orientation, and nanoparticle size [4–6]. Structure-property detailed

analysis and understanding of the physicochemical properties of the oxides are prerequisites to improve their properties and to spur development of new oxide materials.

Among the various process technologies, solution process has many advantages, not only simple and low-cost process but also homogeneity and excellent composition control and high throughput [7]. Oxide solutions are generally synthesized using functional metal precursors in solvents and deposited on substrates by various coating methods. The coated oxide gels were pre-annealed to remove the solvents and post-annealed to develop active layers. Design of metal oxide precursor solutions (metal composition, metal precursor, chelating agents, etc.), treatment of intermediate oxide gels, and annealing techniques are of paramount importance for controlling and improving structural and opto-electronic properties of final oxides.

In this chapter, we review the progress in solution-processed functional oxide thin films produced at a low temperature and highlight the critical challenges for the fundamental understanding and practical implementation of complex oxides in devices.

2. Low-temperature solution-processed oxide dielectric thin films

2.1. Introduction

In this section, we focus on the low-temperature solution deposition of high-quality oxide dielectric thin films for the fabrication of active electronic devices such as thin-film transistors (TFTs). Highly stable oxide dielectric materials are of paramount importance as implemented through sophisticated additive processing with the other components of a TFT. However, compared to vacuum-based deposited oxide films, solution-processed counterparts are generally found to be inferior due to their deposition, metal precursors, morphological characteristics, and performance limitations. Although realizing capabilities to print and integrate solution-processed device-quality oxide dielectrics poses a very significant challenge, success is very likely to open many opportunities in fabricating active electronics as well as in providing new approaches to the production of various unique optical and optoelectronic devices. In addition, solution processing of oxide dielectric thin films at a temperature well below 300°C, which likely opens the door to flexible electronics, has remained challenging. By various approaches including tailoring precursor solution or functional solution chemistry, deposition, annealing/heating profile, activation of amorphous film, such as photo-assisted annealing (UV), solvothermal synthesis, and so on, low-temperature solution-processed oxide dielectric thin films have become possible now.

2.2. Materials selection for oxide dielectrics

Conventionally, silicon dioxide (SiO_2) has been used as dielectric layer in metal-oxide-semiconductor (MOSFET) due to its excellent insulating property and perfect Si/SiO_2 interfacial properties. Advanced technology has enabled fabrication of sub-22 nm channel-length MOSFET, which requires the thickness of SiO_2 to be less than 1 nm [8–10]. However, it is not possible to maintain small leakage currents, which increase dramatically through

http://dx.doi.org/10.5772/intechopen.75610

tunneling for very thin films. In this regard, it is useful to consider the important film features and performance metrics that will produce an optimal gate dielectric. The following are general requirements for a good dielectric film: large relative dielectric constant (>10) and small leakage current density (<10 nA/cm^2 at 1 MV/cm), low-dielectric loss (tanσ < 0.01), and large breakdown field (>4 MV/cm) to preserve the device function as shown in **Figure 1(a)**. In addition, high-mechanical strength, low-thermal expansion, low-water adsorption quality, and high-chemical inertness properties are highly desired. It is worth noting that the transistor mobility strongly depends on the quality of semiconductor/dielectric interface. A dielectric with a rough surface would result in irregular semiconductor/dielectric interface, impeding the flow of charges through the semiconductor. Thus, atomically flat dielectric film surface is essentially required. To achieve the necessary leakage current and breakdown field, films must be as dense as possible and exhibit no pores or cracks. Both from the perspective of surface smoothness and the need for high-breakdown field and low-leakage current, films with amorphous structure are generally preferred for the fabrication of gate dielectric layers.

Because of the challenges in producing such insulators through solution methods, most solution-processed oxide TFTs [11–17] have been fabricated by using binary oxide gate insulators formed through vacuum-based depositions. Although binary oxides will continue to be used for TFT gate dielectric applications, they do not represent an optimal approach to realizing high-performance devices. Generally, binary oxides tend to crystalize [18–20] at relatively low-process temperatures, resulting in enhanced impurity interdiffusion and high-leakage currents due to formation of grain boundaries. Two most important prerequisites of oxide

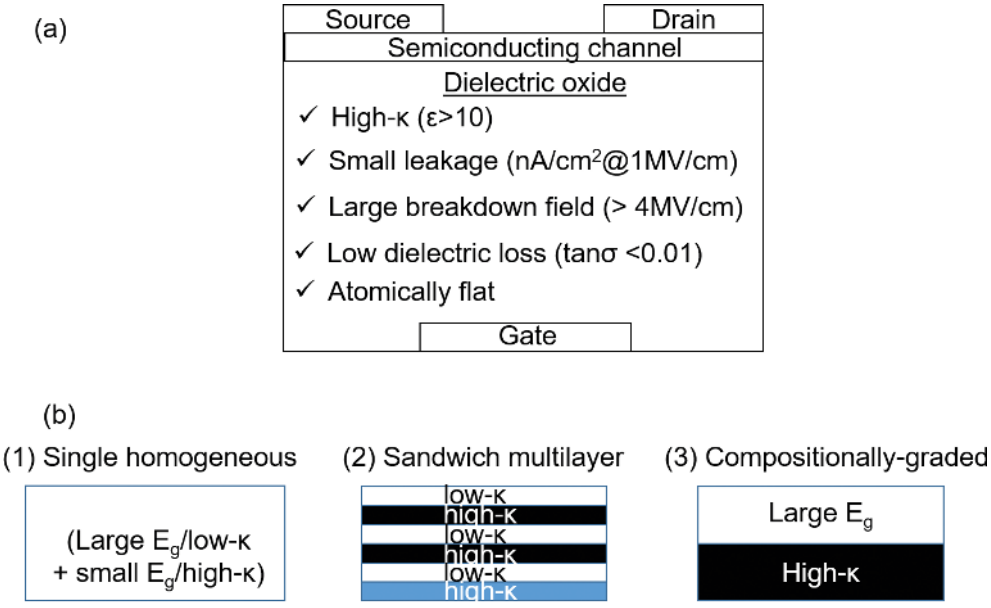

Figure 1. (a) General requirements of a dielectric layer and (b) major designs of device-quality dielectric layer.

dielectrics are high-dielectric constant and large breakdown field [21]. However, selection of a binary oxide as an insulator generally involves a compromise between these two characteristics. That is because binary oxides with high-dielectric constants normally have small band gaps (HfO_2, Ta_2O_5, ZrO_2, La_2O_3, and TiO_2) and vice versa (SiO_2 and Al_2O_3).

One approach to the production of high-performance dielectrics relies on the use of mixed multiple-component oxides. These oxides provide convenient means for controlling the dielectric constant and breakdown field through incorporation of components that specifically contribute to either dielectric constant or breakdown. Furthermore, amorphous phase can be stabilized by mixing multi-components, resulting in the films with extremely flat surfaces. Common binary oxides used for tuning these properties are listed in **Table 1** [20, 22–26].

To meet the performance requirements of gate dielectrics in TFTs, multi-component oxides can be produced by strategies as illustrated in **Figure 1(b)**. A single homogeneous dielectric can be produced by combining selected wide band-gap materials with those exhibiting smaller gaps and higher dielectric constants. For example, the mixtures of Hf-Si-O [27–29] and HfO_2-Al_2O_3 [30, 31] have been extensively studied as gate dielectrics in Si CMOS devices. Alternatively, wide- and small-gap materials can be interleaved to form multilayered structures, as demonstrated by stacked layers of TiO_2 and Al_2O_3 produced through atomic layer deposition. The presence of sharp dielectric interfaces in such structured materials provides a means to improve dielectric-breakdown fields. Finally, a compositionally graded material dominated by a high-dielectric-constant material at the metal-insulator interface and a high-band-gap material at the dielectric-semiconductor interface provides an additional alternative.

2.3. Producing high-quality films from solution

The fundamental challenges in depositing oxide thin films from solution are associated with the processes of conversion of soluble precursors into dense solids. Thus, understanding the structure of metal-organic precursors in solution and their effects on processability and on the final structure and properties of the oxide is the key to the production of high-quality oxides. Although improvements of solution-processed oxide dielectrics reported so far are impressive, many of them exhibit porous structures with coarse morphologies indicating that proper

Material	κ	E_g (eV)	CBO (eV)	VBO (eV)
SiO_2	3.9	9.0	3.2	4.7
Al_2O_3	9.0	8.8	2.8	4.9
La_2O_3	30	6.0	2.3	2.6
ZrO_2	25	5.8	1.5	3.2
HfO_2	25	5.8	1.4	3.3
Ta_2O_5	22	4.4	0.35	2.95
TiO_2	80	3.5	0	2.4

Table 1. Summary of some relevant characteristics of major binary oxides.

chemistries have not been utilized. By placing greater emphasis on conversion pathways from precursor to oxide, low-energy reactions should be devised that allow condensation to proceed uniformly. Especially for electronic applications, thin oxide films must retain density, homogeneity, and uniformity during condensation.

It was found that *hybrid clusters, having inorganic cores coordinated by organic ligands*, are the typical form of metal-organic precursor structures [32]. The study has shown that solvothermal synthesis of the precursor results in significantly improved insulating properties (e.g., two orders lower leakage current) of high-temperature annealed oxide films. We put emphasis on the structural analysis of the cluster precursors and annealed solids and relate the results to the significant improvement of properties by solvothermal treatment of solutions. A change in the cluster core toward structural unification can be brought about by the solvothermal treatment, leading to higher uniformity and higher stability of clusters. The final structure of the material maintained the features of the core structure in solution, even after annealing at high temperatures. These results demonstrate the key role played by designing cluster structure in solution. In addition, improved synthesis of the cluster precursor under solvothermal conditions leads to low-temperature deposition of oxide insulating films at below 200°C. Based on these strategies, we have designed and succeeded in producing various high-quality oxide dielectric films including lanthanoids-zirconium-oxide systems (Ln-Zr-O, Ln = La, Ce, Nd, Sm, Gd, Ho, Tm), Hf-Zr-O, Y-Zr-O, Hf-Ta-O, La-Ti-O, and Hf-La-O. As a typical example, detailed studies on La-Zr-O system will be shown in the following part with a focus on the structural analysis of the cluster precursor under solvothermal conditions.

2.3.1. Hybrid cluster precursors of the La-Zr-O insulator for transistors

Both lanthanum oxide and zirconium oxide are typical high-κ materials, having dielectric constant values in the range of 20–30. However, lanthanum oxide is hygroscopic, and both oxides are polycrystalline. Addition of Zr to La-O to create insulating LZO system with a dielectric constant in the range of 20–25 exhibits diverse chemistries in solution and resists crystallization in the solid phase. The LZO dielectric has shown some excellent properties in all-oxide TFTs [33–35], but leakage needs to be further suppressed and a processing temperature that is compatible with plastic substrates is highly desirable. Analyses of structures of solutions, gels, and solids by various characterizations have revealed a close structural relationship between the clusters in the solutions and the final solids even after annealing at high temperatures [32].

The synthesis of LZO precursor solution is summarized in **Figure 2**. First, lanthanum (III) acetate (La(OAc)) and zirconium (IV) butoxide solution (Zr(BtO)) were each dissolved in appropriate amounts of propionic acid (PrA) to produce La and Zr solutions. After that, the two solutions were mixed to obtain LZO mixtures with La/Zr molar ratios of 3/7 (LZ37) or 5/5 (LZ55). For solvothermal treatment, the LZO mixtures were sealed in an autoclave (AC) container and heated at 160–180°C for 2–5 h with magnetic stirring. The precursor solutions were spin coated on Pt/Ti/SiO_2/Si substrates, followed by annealing at 200–500°C in oxygen.

The thermal behaviors of precursor solutions were analyzed by thermal-gravity differential thermal analysis (TG-DTA) (**Figure 3**). Comparing LZO solutions with and without solvothermal treatment, we have observed three key features: (1) the decomposition

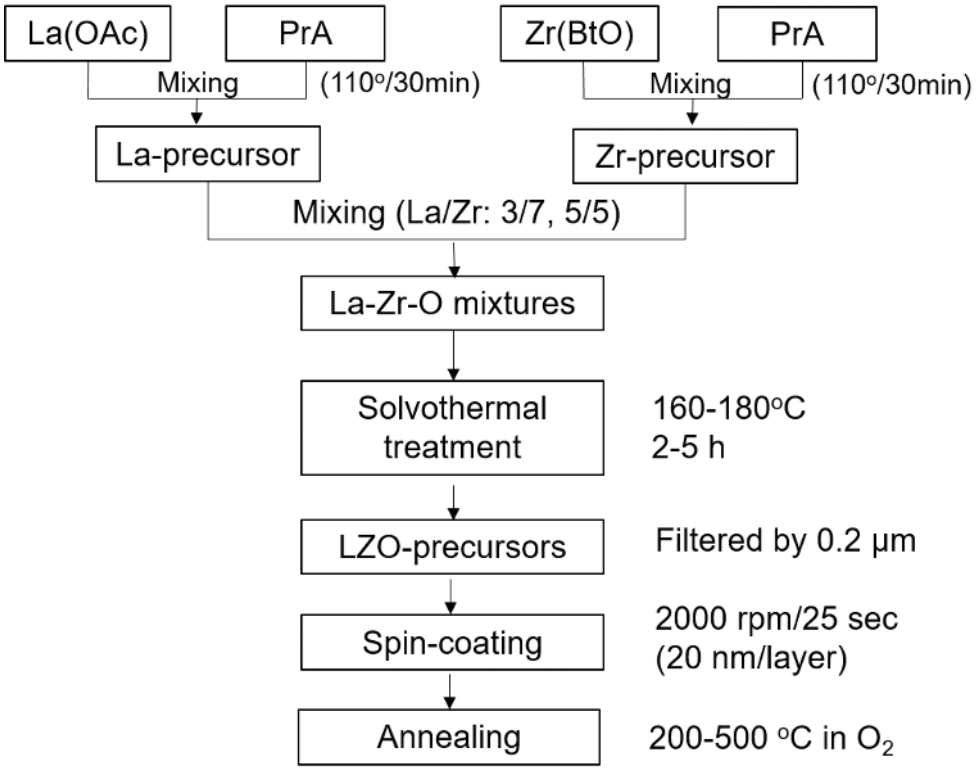

Figure 2. Schematic diagram of synthesis of the LZO precursor solution.

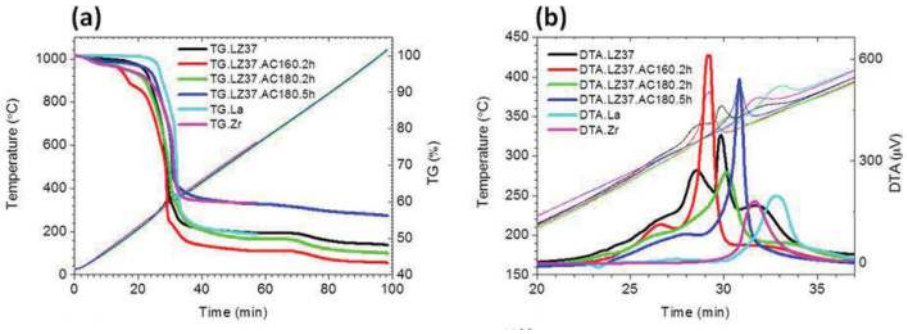

Figure 3. TG-DTA analyses of different LZO precursors solution.

temperature of the organic components was affected by the solvothermal treatment, i.e., evolution from multiple, different cluster structures toward a single cluster structure, leading to a more uniform and stable cluster structure. (2) Both the La-only and Zr-only precursors

showed decomposition temperatures higher than those of LZO precursors, indicating that the La and Zr components were not simply mechanically mixed, even before solvothermal treatment. (3) The residual masses after TG analysis were quite different for solvothermally treated precursor solutions, representing the variation in the inorganic and organic contents in the precursors. Therefore, we speculate that the cluster development underwent two stages. The first stage is likely to be associated with the decomposition of the initial Zr clusters during their transition into La-Zr clusters. The second stage involved further growth/condensation of the clusters.

Interestingly, the solvothermal treatment impacted not only on the solution structure but also on the final material structure. It was turned out that solvothermal treatment led to a uniform structure in the precursor, which was even inherited by the final annealed oxide. Without pre-formation of a uniform cluster structure, the final material remained non-uniform even if the metal components in the precursors were well mixed on the cluster scale but not inside the clusters. This suggests that the inorganic core of the cluster in the precursor remained the structural unit after annealing, during which the organic ligands around it decomposed and the cores compacted, without significantly reacting with the surrounding components. Therefore, the solvothermally treated La-Zr solutions resulted in more uniform oxide solids with improved insulating and dielectric properties. The reorganization of the clusters under solvothermal conditions also enhanced UV light absorption and enabled film deposition under UV light at low temperature, which is presented in more detail in the following part.

2.3.2. Lowering processing temperature for the La-Zr-O dielectric

As mentioned earlier, a cluster core containing two or more metal elements with a structure similar to that of desired final oxide can be used as a building block for film deposition. In this method, the preferential decomposition of one metal compound over the others that causes compositional segregation is not expected to occur because the different metal elements have already been combined into one core and thermal dynamically stabilized. Hence, the decomposition and densification are similar to those occurring in binary metal oxide system. The structure of the clusters, as well as their uniformity and stability, influences the insulating properties of low-temperature deposited film.

The solvothermally treated solutions were found to have a highly enhanced UV absorption ability because of the structural reorganization of the cluster cores, which may facilitate the decomposition of their organic ligands under UV irradiation. The LZ37 films UV-annealed at 200–300°C had densities in the range of 4.3–4.5 g cm^{-3}, which corresponds to only 70–74% of the density of LZO crystals. An excellent insulating ability (~10^{-8} A cm^{-2} at 2 MV cm^{-1}) of the film was achieved (**Figure 4(b)**). Without solvothermal treatment of the solution, the current density is several orders higher, indicating significant effect of solvothermal treatment on the improvement of the film properties. In addition to the improvement of the cluster core, the solvothermal treatment of solutions also enhances the organic ingredient to be stabilized by the UV annealing, which facilitates formation of C—O bonding. Improvements of both the cluster core and the organic ingredient greatly contribute to the enhanced dielectric properties of LZO films.

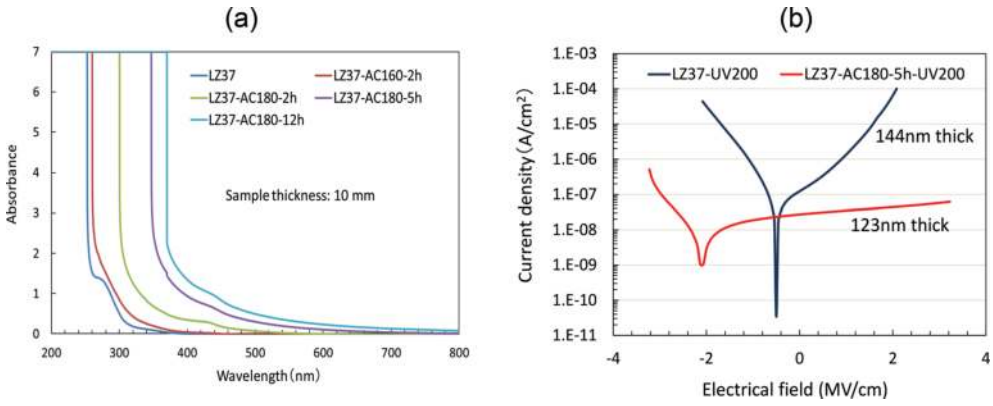

Figure 4. (a) UV-vis absorption spectra of LZO precursor solutions and (b) eakage currents of LZO films with and without solvothermal treatment.

Finally, using the LZ37 film UV/O_3-annealed at 200°C, we fabricated a TFT with a bottom-gate top-contact structure. The TFT exhibited a low-gate leakage current of less than 10 pA at an operating voltage of 15 V, a large "on/off" ratio of near 10^6, a field-effect mobility (μ) of 0.37 $cm^2\ V^{-1}\ s^{-1}$, and a subthreshold swing factor (*SS*) of 0.61 V $decade^{-1}$. The off current of the drain (3–30 pA) and the gate leakage (~10 pA) were extremely low and comparable to those of TFTs with the thermally grown SiO_2 insulator [36], indicating excellent insulating property of the low-temperature-processed LaZrO. The *SS* value is similar to those of high-temperature-processed In-Zn-O/LaZrO [35] and In-Zn-O/SiO_2 (channel/gate insulator) TFTs, suggesting the similar channel/gate insulator interface properties.

3. Low-temperature solution-processed oxide semiconductor thin films and transistors

3.1. Introduction

Inorganic semiconductors including silicon and chalcogenides have been solution-processed into high-performance semiconductors that have better mobility (>10 $cm^2\ V^{-1}\ s^{-1}$) and stability in comparison with organic semiconductors [37, 38]. These solution-processed inorganic semiconductors, however, generally require high annealing temperature, necessary for generating crystalline phases, impurity-free, and dense structures for device-quality films.

On the contrary, in oxide semiconductors, the amorphous phases are capable of exhibiting electron mobilities comparable to those of their crystalline phase counterparts [39–41], which allow the exclusion of a high-temperature annealing process for obtaining crystalline phases. The conduction band minimum (CBM), which constitutes the electron conduction pathway, is composed of vacant metal cation s-states, and the spatial expanse of these s-states is greater than the inter-cation distances. The s-state spatial overlap is primarily determined by the principal

quantum number (n), and therefore, heavy post-transition metal cations with $(n–1)d^{10}$ ns^o electronic configurations, where $n \geq 5$, are ideal oxide semiconductor candidates [42]. Both In^{3+} and Sn^{4+}, which have the same $[Kr](4d^{10})5s^o$ electronic configuration, meet this requirement, and a highly dispersed CBM is also found in ZnO due to the small interaction distances [43]. To date, most amorphous oxide semiconductors (AOSs) are deposited on rigid substrates, such as glass and metal foil, and are processable at a high temperature (>400°C). Recent efforts to lower the annealing temperature have shown that device-quality AOSs, exhibiting high performance and device stability that are not easily achievable in organic semiconductor-based electronics, have been successfully grown on plastic substrates. In the following part, we summarize the recent advances in the development of solution-processed AOS at a low temperature. In particular, we discuss the chemical pathways (colloidal-based process, sol-gel routes, auto-combustion chemistry, and impurity-free precursor-based approach) and physical approaches by newly developed annealing techniques (photo-assisted, microwave, and high pressure), which effectively enable the fabrication of low-temperature, solution-processable, high-performance AOS-TFTs.

3.2. Approaches to low-temperature solution-processed AOS-TFTs

3.2.1. Chemical pathways

3.2.1.1. Nanomaterials-based process

The nanoparticles (NPs)-based chemical approach is, in principle, the promising pathway for low-temperature annealed, high-performance semiconducting layers. Nevertheless, whereas the metal NPs, smaller than a few tens of nanometers, can be melted even below 200°C due to the dramatic lowering of the melting point [44, 45], the oxide NPs are not capable of undergoing the structural transformation into a granular film morphology at low temperatures, since the melting point of oxide NPs is not decreased depending on the particle size. This unique physical property of oxide NPs leads to the large surface area, porous, and poorly interconnected particulate film at low annealing temperatures, which limits device performance (low mobility and poor stability). For example, In_2O_3 NPs, less than 10 nm in size and spherical in shape, have been generated through chemical synthesis and implemented into device structures by ink-jet printing even at room temperature. However, the μ was confined to 0.8 cm^2 V^{-1} s^{-1} [46–48], which is associated with the inefficient carrier transport at junctions between neighboring NPs.

3.2.1.2. Sol-gel chemistry

In metal salt-based sol-gel chemistry, the precursor solution is synthesized by dissolving metal salt precursors in solvents with stabilizing agents and water. The resulting metal complexes undergo a hydrolysis reaction through the loss of a proton by one or more of the water molecules that surround the metal cations in the first solvation shell. As a consequence, the aquo ligand molecule, water, bonded to the metal cation is transformed into either a hydroxo ligand, OH^-, or an oxo ligand, O^{2-}. Subsequently, a condensation reaction occurs due to the oxolation generating an oxo-bridge, M-O-M, allowing the formation of a metal oxide skeleton framework with a dense microstructure.

Elimination of impurities such as hydroxides, anions, and carbon along with the formation of oxygen vacancies is critical for determining properties of AOS because they not only hinder the sol-gel oxide framework formation reaction but also interrupt the efficient transport of charge carriers [49]. To enable low-temperature processable products, the thermal decomposition of metal precursors should be completed at a low temperature, as evidenced by the use of metal nitrate precursors, the anion of which is almost completely decomposed even at 250°C, instead of other metal precursors (chloride, acetate) [50]. In addition, the chemical structure should be tailored toward a framework containing less hydroxide, which can be realized by doping an element that has a high electronegativity [51].

A "sol-gel on chip" hydrolysis approach from soluble metal alkoxide precursors was reported [52], which affords unprecedented high μ of ~10 $cm^2 V^{-1} s^{-1}$, reproducible and stable turn-on voltage (~0 V) at maximum process temperature as low as 230°C. The approach uses the *in-situ* hydrolysis and condensation of transition metal alkoxides when they are exposed to an aqueous environment by nucleophilic substitution, thus affording the M-O-M framework at low temperature. The process is applicable to a broad range of AOS that are of immediate interest in TFT applications.

3.2.1.3. Impurity-free precursor-based approach

The presence of impurities has a negative impact on the performance of oxide semiconductors. In this regard, the metal-hydroxide nanocluster is a viable alternative to metal-salt precursors due to the absence of impurity-containing chemical species. The metal hydroxide is converted into a metal oxide framework by a thermally activated reaction. Aqueous Zn hydroxide solution was shown to drastically lower the annealing temperature to 150°C, producing ZnO-TFT with a μ of 0.4 $cm^2 V^{-1} s^{-1}$ [53]. Another approach for the impurity-free precursor is the use of aqueous carbon-free metal-oxide precursors such as zinc oxide hydrate dissolved in ammonium hydroxide to generate Zn ammonium complex precursor [54]. This route allows for the growth of ultra-thin (4–5 nm), high-quality polycrystalline ZnO films on arbitrary substrates. Transistors fabricated using this simple process at 180°C showed an electron mobility of up to 11.0 $cm^2 V^{-1} s^{-1}$.

Formation of the ammine-hydroxo complex and its low-temperature conversion to corresponding oxide, however, are generally not convenient, except for Zn. Thus, the design of a new chemical complex with the easy accessibility to other elements and the low-temperature processability for chemical transformations are essential in the impurity-free precursor-based approach.

3.2.1.4. Auto-combustion synthesis

A redox-based combustion synthetic approach was applied to oxide thin films using acetylacetone or urea as a fuel and metal nitrates as oxidizers [55]. The self-energy-generating combustion chemistry provides a localized energy supply, eliminating the need for high, externally applied processing temperatures. Furthermore, the atomically local oxidizer supply can efficiently remove organic impurities without coke formation in combustion reactions with balanced redox chemistry. The semiconducting In_2O_3 annealed at temperature as low as 200°C yielded TFTs with μ approaching 1.0 and 13.0 $cm^2 V^{-1} s^{-1}$ on SiO_2 and Al_2O_3 gate dielectrics, respectively.

3.2.2. Physical pathways

3.2.2.1. Microwave annealing (MW)

The use of microwave-assisted annealing enabled quick fabrication of ZnO-TFT at 140°C with a μ of 1.7 $cm^2 V^{-1} s^{-1}$, which is improved to three- to sixfolds in comparison with TFTs processed by conventional hot-plate annealing [56]. This enhanced TFT performance is attributed to the improved development of ZnO grains suitable for reducing the length of transport paths across grain boundaries and the shorter Zn-Zn distance enabling better overlap between the Zn s-orbitals, thus creating chemical structures appropriate for high-performance AOS.

3.2.2.2. Deep-ultraviolet assisted annealing (DUV)

Much efforts have also been focused on the treatment of sol-gel films by photochemical activation using deep-ultraviolet (DUV) irradiation [36, 57–61]. When the as-deposited film is exposed to DUV irradiation, high-energy DUV photons induce photochemical cleavage of alkoxide groups and activate metal and oxygen atoms to facilitate M-O-M network formation (**Figure 5**, step 1, condensation). Further irradiation induces a gradual removal of oxygen and carbon (and, thereby, near-complete condensation) and a transition to a film densification (**Figure 5**, step 2, densification). This DUV technique is applicable to numerous AOS. The μ of the room temperature DUV-IGZO is as high as 14.0 $cm^2 V^{-1} s^{-1}$.

3.2.2.3. High-pressure annealing (HPA)

HPA influences thermodynamics of solution-processed AOS films, facilitating denser film formation by reducing its thickness under a high pressure (2 MPa). In addition, high-oxygen pressure changes the Gibbs free energy of the system and strengthens the bonding between metal ions and oxygen. As a result, TFT processed at 220°C exhibited a μ of 1.7 $cm^2 V^{-1} s^{-1}$ and high-bias stability [62].

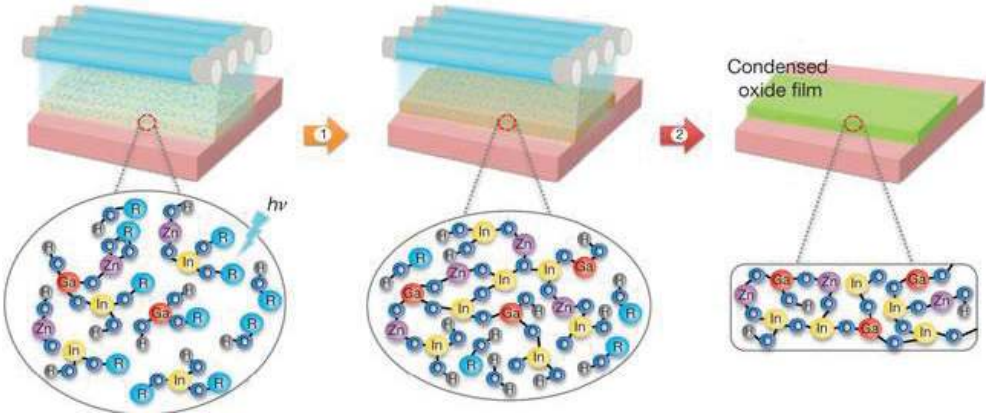

Figure 5. Schematic diagram for the condensation mechanism of metal-oxide precursors by DUV irradiation.

3.2.2.4. Laser-assisted annealing

A femtosecond (fs) laser annealing was applied for an effective and rapid fabrication of AOS thin films [63]. The method led to improvements in μ (9.0 $cm^2 V^{-1} s^{-1}$) and in "on/off" ratio due to the efficient removal of impurities and enhanced metal-oxide composition.

A summary of solution-processed AOS-TFTs fabricated at a low temperature (<300°C) is given in **Table 2**.

3.3. Conclusions and outlook

During the past decade, there has been significant active research regarding the development of high-performance semiconductors that can be generated by a low-cost, large-scale solution process. The recent progress with solution-processed, high-performance AOS confirms their potential feasibility in electronic applications. For practical realization of high-performance electronic devices even on plastic substrates, the high mobility at annealing temperature below 150°C

Precursor type	Semi.	Ann. temp. (°C)	Insulator	Mobility ($cm^2 V^{-1} s^{-1}$)	On/off	Note
Nanoparticle	In_2O_3	RT	—	0.8	2×10^3	Colloidal [48]
Nanorod	ZnO	230	SiO_2	0.6	$<10^6$	Colloidal [64]
Ammine-hydroxo	ZnO	150	SiO_2	0.4	10^6	Impurity-free [53]
Ammonia complex	Li-ZnO	300	SiO_2	11.45	10^7–10^8	Alkali doping [65]
Metal salt + fuel	In_2O_3	200	Al_2O_3	13.0	10^3	Combustion [55]
			SiO_2	1.0	10^5	
Alkoxide	IZO	210	Al_2O_3	6.0	10^8	Sol-gel on chip [52]
Metal salt	In_2O_3	300	SiO_2	22.1	10^5–10^6	O_2/O_3 anneal [66]
		200		0.85		
Hydroxo	ZnO	140	SiO_2	1.7	10^7	MW [56]
Metal nitrate	In_2O_3	140	Al_2O_3	2.0	10^8	Precursor soaking [67]
Metal salts	IGZO	<80	Al_2O_3	8.76	10^8–10^9	DUV [36]
	In_2O_3			11.29		
Metal nitrate	In_2O_3	180		3.2	$>10^6$	Far UV [68]
		200		7.5		
Aqueous carbon-free	ZnO	80–180	Al_2O_3/ZrO_2	11.0	10^4–10^5	DUV [54]
Metal salt	IZO	220	SiO_2	1.78	10^6	HPA [62]
Metal salt	IZO	—	—	9.0	—	Laser anneal [63]

Table 2. Summary of low-temperature (<300°C) solution-processed oxide semiconductors.

is an inevitable requisite, which is considered achievable in solution processable AOS when the chemical/physical challenges addressed. The development of new chemical precursors for impurity-free AOS, the incorporation of dopants that can improve the electrical characteristics, and bias stability, and advanced annealing techniques for the generation of high-quality AOS would significantly improve the electrical performance of AOS processed by a solution process at a low temperature, thus making various practical electronic applications possible.

4. Conducing oxide thin films prepared from low-temperature solution processing

4.1. Transparent conducting oxides (TCOs) in general

The use of highly conductive and highly transparent thin films in the visible range of the spectrum is of great importance for a variety of optoelectronic device applications such as displays, solar cells, opto-electrical interfaces, and circuitries. Transparent conducting oxides (TCOs), in contrast to glass fiber, silicon, and compound semiconductors, are highly flexible intermediate states, whose conductivity can be tuned from insulating through semiconducting to conducting as well as their transparency adjustable. Furthermore, main carriers can be switched between n-type and p-type, opening a wide range of new technological applications.

So far, TCOs including binary, ternary, and quaternary oxide systems are mainly based on indium (III) oxide (In_3O_3), tin (IV) oxide (SnO_2), zinc (II) oxide (ZnO), and their mixtures with some dopants to tune structural and opto-electrical properties (**Figure 6**). The plot of In_2O_3 includes results for Sn-doped c (ITO) and other dopants, and the plot for various deposition methods is shown in **Figure 7** [69]. The slopes of the plots for improvement versus time in lowering doped In_2O_3 and doped SnO_2 resistivities appear to plateau at approximately 10^{-4} and 2×10^{-4} Ω cm, respectively. Thus, it is likely that further technological improvement in lowering resistivity of these materials is limited. However, the doped ZnO plot still presents a descending slope of improvement versus time. Therefore, it can be considered that further improvement of conductivity of ZnO-based systems would be possible.

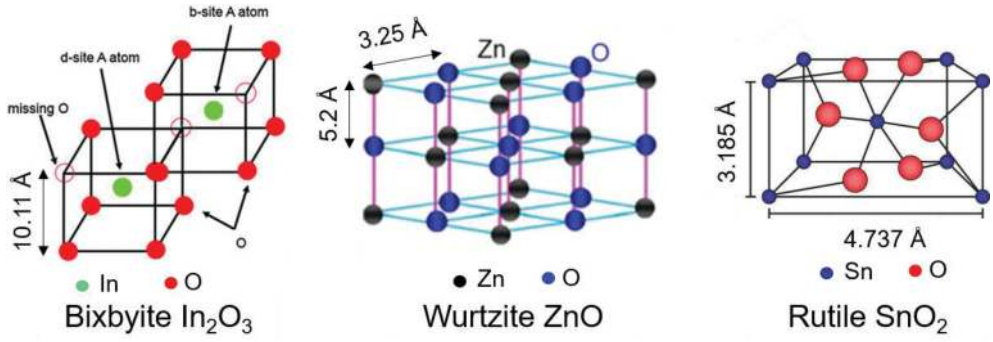

Figure 6. Unit structure of typical binary oxides: bixbyite In_2O_3, wurtzite ZnO, and rutile SnO_2.

4.2. N-type conductive oxides

4.2.1. Indium-tin-oxide (ITO)

ITO is the most widely used TCOs because of its two key characteristics: conductivity and optical transparency. Conventionally, ITO films are produced by vacuum-based deposition techniques. The best resistivity of ITO film deposited by sputtering was reported as low as 1.2×10^{-4} Ω cm [70]. As an alternative to vacuum-based deposition, recently much efforts have been focused on production of solution-based deposition for high-performance ITO films using various approaches such as nanomaterials-based [71–75], aqueous metal salts solution [76], combustion synthesis [77, 78], and advanced annealing techniques (microwave annealing [79] and ultraviolet laser annealing [80]. A summary of properties of ITO films prepared by various solution-based deposition processes is given in **Table 3**.

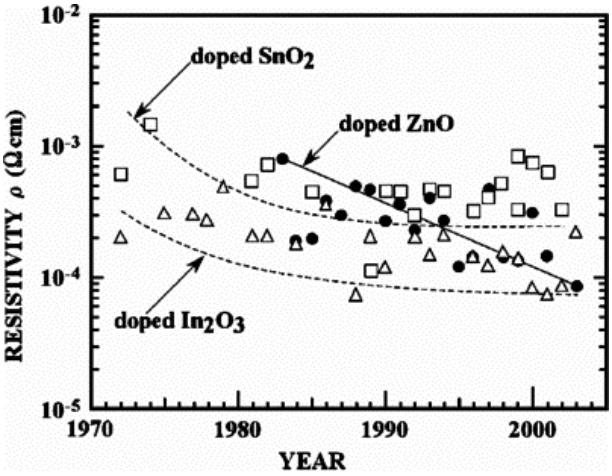

Figure 7. The plot of resistivity improvement versus time for various TCOs.

ρ (10^{-4} Ω cm)	R_s (Ω)	t (nm)	T (%)	Φ_H (10^{-2} Ω^{-1})	Deposition	Ref
45.7	47.5	144	85.3	0.420	Electrospray	[79]
42.3	188	225	80	—	Dip coating	[76]
2.5	42	60	~85	0.469	Dip coating	[81]
2.1	7.1	295	~78	1.171	Dip coating	[82]
310	—	75	>90	—	Spin coating	[80]
0.52	356	146	93	0.136	Spin coating	[74]
4.2	81	70	—	—	Spin coating	[77]
7.2	30	241	90.2	1.191	Spin coating	[72]

Table 3. Properties of ITO films prepared by various solution-deposition processes.

A redox-based combustion synthetic approach was applied to ITO thin film using acetylacetone as a fuel and metal nitrate as an oxidizer, which enabled production of high-quality ITO film at a temperature as low as 250°C [77]. The redox reaction between the fuel and oxidizer in the precursor solution generates internal heat, facilitating conversion from metal precursor to metal oxide at low temperature. The SCS-ITO thin film exhibited high-crystalline quality, atomically smooth surface (RMS ~ 4.1 Å), and low-electrical resistivity (4.2×10^{-4} Ω cm). The TFT using SCS-ITO film as the S/D electrodes showed excellent electrical properties with negligible hysteresis. The obtained "on/off" ratio, *SS*-factor, V_{th}, and μ were 5×10^7, 0.43 V/decade, 0.7 V, and 2.1 $cm^2 V^{-1} s^{-1}$, respectively (**Figure 8**). The performance and stability of the SCS-ITO TFT are comparable to those of the sputtered-ITO TFT, emphasizing that the SCS-ITO film is a promising candidate for totally solution-processed oxide TFTs.

4.2.2. Alternatives to ITO

There are increasing emphases on not only developing a TCO with higher conductivity but also with a material other than ITO. Two major concerns with ITO are the cost and the potentially limited resource.

Current candidate materials for a higher conductivity TCO are summarized in **Table 4**, which include the conventional binary oxides of CdO, SnO_2, In_2O_3, and ZnO, with alternative dopants, and combinations of these binaries, plus Ga2O3, in ternary, quaternary, and even quinary combination of these five oxides.

As a promising binary TCO material, ZnO is considered the prime candidate for a higher conductivity and to be low cost. However, ZnO is more sensitive to oxygen than ITO, and process control is more difficult. Work continues on improving ZnO with alternative dopants, especially Al (AZO) and Ga (GZO). As for sol-gel AZO film, the lowest reported resistivity is 1.5×10^{-4} Ω cm [83], which is close to that of film prepared by sputtering [84].

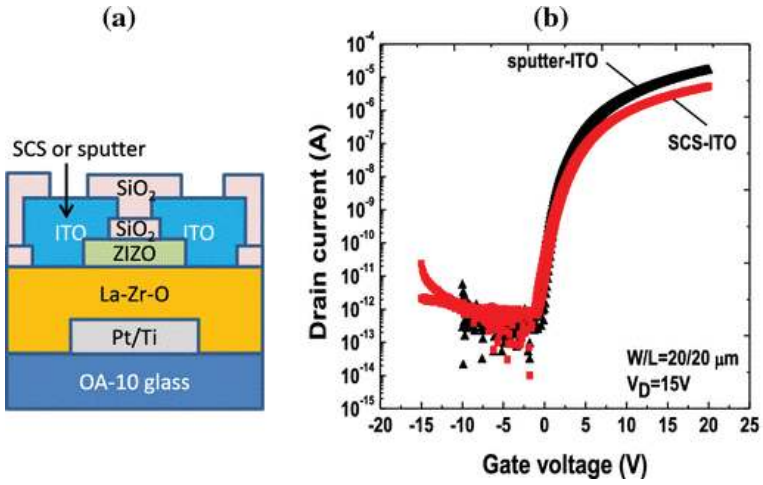

Figure 8. (a) Cross-sectional structure and (b) transfer curves of ZIZO-TFT using SCS-ITO as S/D electrodes.

Material	Dopant or compound
In_2O_3	Sn, Ge, Mo, F, Ti, Zr, Hf, Nb, Ta, W, Te, Mg
SnO_2	Sb, F, As, Nb, Ta
ZnO	Al, Ga, B, In, Y, Sc, F, V, Si, Ge, Ti, Zr, Hf
CdO	In, Sn
ZnO-SnO_2	Zn_2SnO_4, $ZnSnO_3$
ZnO-In_2O_3	$Zn_2In_2O_5$, $Zn_3In_2O_6$
Ga-In-O	Sn, Ge
$CdSb_2O_6$	Y
Cd-In-Sn-O	$CdIn_2O_4$-Cd_2SnO_4

Table 4. Conductive oxides based on multinary metal oxide systems other than ITO.

4.3. P-type conductive oxides

Highly conductive p-type oxides serve as critical components for various technological developments such as efficient charge injection layers for light-emitting devices [85], solar cells with better band-matching current collectors [86, 87], invisible circuits, and applications in near-infrared optoelectronics where n-type TCOs provide poor optical transmission. In contrast to widespread use of n-type TCOs such as ITO, p-type TCOs have not been commercialized yet due to their significantly low-carrier mobility and electrical conductivity. In fact, research toward p-type amorphous TCOs is highly challenging even by using vacuum deposition techniques, which result in very limited materials: Zn-Rh-O (resistivity 0.5 Ω cm) and Zn-Co-O (0.05 Ω cm). The difficulties originated from electronic structure of p-type TCOs, which exhibits the strong localization of the upper edge of the valence band to oxide ions.

The Hosono group has initiated breakthrough research toward p-type oxides. They found a series of transparent p-type Cu oxides with delafossite structure such as $CuGaO_2$ and $CuAlO_2$ [41, 88–90], and amorphous Zn-Rh-O, Zn-Co-O systems [41, 88, 91]. However, most of these p-type TCOs were produced by vacuum-based deposition techniques. Solution-processed p-type conductive oxides have remained very challenging.

Recently, misfit-layered $Ca_3Co_4O_9$ thin film synthesized through solution processing is shown to be high-performing p-type TCOs [92]. The synthesis method consists of sol-gel chemistry, spin coating, and heat treatment at 650°C. A resistivity and visible range transparency of 57 mΩ cm and 67%, respectively, were obtained. However, the required high-annealing temperature over 600°C may limit its practical uses.

In order to produce conductive amorphous p-type oxides from solution at low temperature, we focused on Ru oxides [93]. Crystalline RuO_2 is a well-known electrode material that exhibits metallic conduction. Initially, we found that the amorphous phase of RuO_2 is unstable, and only crystalline phase can be obtained through solution processing even at a low temperature

below 300°C. We then used lanthanide elements (Ln, except Ce) to stabilize the amorphous phase. As a result, we found a series of solution-processable amorphous p-type conductive Ln-M-O (a-Ln-M-O, where M = Ru, Ir, and Ln is lanthanide elements except Ce) having low resistivity (10^{-3}–10^{-2} Ω cm) (**Figure 9**). The resistivity increases with increasing Ln atomic number (Z) and changes evidently faster for Z > 64 (Gd), which may be more related to the influence of 4f electrons (4f subshell is more than half-filled at Z > 64) than to the decreasing size of Ln ions. These oxides are thermally stable to a high degree, being amorphous up to 800°C, and processable below 400°C. These oxides have three pronounced features: first, their valence electrons have open-shell configurations (t_{2g}^4 in Ru 4d and t_{2g}^5 in Ir 5d), which is distinctively different from the closed-shell or pseudo-closed-shell configurations in other p-type oxides (e.g., Cu $3d^{10}s^0$ in Cu oxides, Sn $5s^2$ in SnO, Rh t_{2g}^6 in Zn-Rh-O, and Co t_{2g}^6 in Zn-Co-O). Second, the conduction of amorphous La-Ru-O (semiconducting) is completely different from that of crystalline phases (e.g., $La_3Ru_3O_{11}$ and $La_4Ru_6O_{19}$, which are both metallic). Third, the resistivity of solution-processed a-La-Ru-O is lower than that of the sputtered sample. Hence, detailed understanding of the electronic structure of these materials and the mechanism underlying processing-composition-conduction correlation is of fundamental importance for future research.

The unique properties of amorphous p-type oxides have high potential for use in printed electronics, e.g., as gate electrode in n-type oxide TFTs [33, 94], and may be modified to use as p-channel in TFTs or as an active layer in solar cells. The narrow band-gap is advantageous for light absorbing in solar cells. The electronic configurations of these amorphous oxides are apparently not analogous to those of known p-type oxides. This deserves theoretical investigation and suggests that more p-type amorphous oxides are ahead of us.

It is known that the conduction of ruthenium pyrochlore, $A_2Ru_2O_7$, is sensitive to the type of A element. These compounds are semiconducting for A = Y and the lanthanides Pr-Lu, and weakly metallic for A = Bi and Pb. The Ln of the aforementioned oxides was thus replaced with Bi and Pb, leading to low-resistivity amorphous oxides produced at low

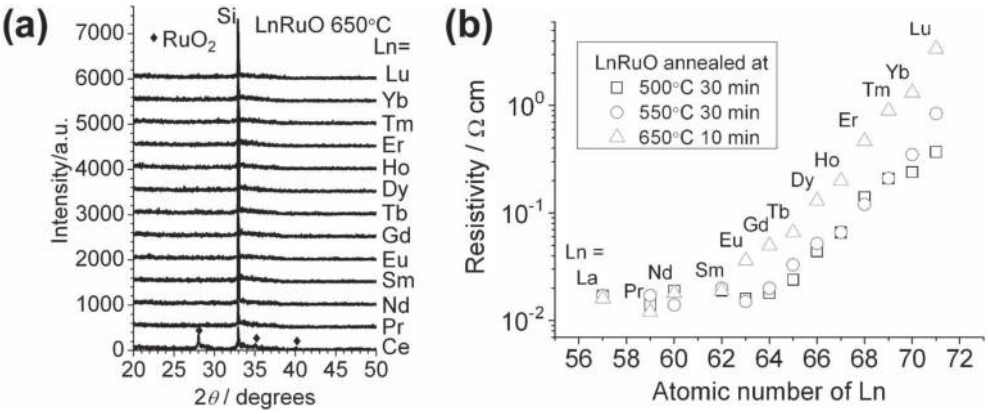

Figure 9. (a) XRD patterns and (b) resistivity of LnRuO films.

Material	Method	T (°C)	ρ/σ	μ ($cm^2 V^{-1} s^{-1}$)	E_g (eV)	Ref.
$CuAlO_2$	So-gel	900	250 Ω cm	—	—	2002 [92]
$CuCrO_2$, $CuAl_{0.5}Cr_{0.5}O_2$	Sol-gel	600	11–16 Ω cm	—	—	2009 [96]
$CuFeO_2$	So-gel	700	0.36 S cm^{-1}	0.7	3.05	2012 [97]
$CuCrO_2$:Mg	CSD	600	0.31 Ω cm	0.7		2012 [98]
Ln-M-O (M = Ru, Ir, and Ln is a lanthanide)	CSD	<400	10^{-3}–10^{-2} Ω cm	—	—	2012 [93]
A-B-O (A = Bi, Pb; B = Ru, Ir)	CSD	240	1.3–3.8 mΩ cm	—	0.2	2012 [95]
$Ca_3Co_4O_9$	CSD	650	57 mΩ cm	—	—	2014 [92]
$CuCrO_2$	Combustion	180	0.14 S cm^{-1}	0.23	3.0	2018 [99]
$CuCrO_2$	Spray pyrolysis	345	12 S cm^{-1}	6.4×10^{-3}	2.4	2015 [100]
Y:$CuAlO_2$	Electro-hydrodynamic	1100	580 Ω cm	–	–	2015 [101]
Li:ZnO		500	15.06 Ω cm	0.918	–	

Table 5. Electro-optical characteristics of some solution-processed p-type conductive oxides.

temperatures [95]. The lowest necessary temperatures for a-BiRuO, a-PbRuO, and a-BiIrO were 240, 290, and 350°C, respectively, resulting in RT DC resistivities of 3.8, 1.7, and 3.8 mΩ cm, respectively. The resistivity of a-BiRuO film has nearly reached the value of crystalline bulk $Bi_3Ru_3O_{11}$ (1.4 mΩ cm), which suggests that the films are of high quality. In p-type oxides, the low-resistivity values of these amorphous oxides are matched only by epitaxial LaCuOSe:Mg annealed at a high temperature of 1000°C (1.1 mΩ cm). A summary of electro-optical characteristics of some solution-processed p-type conductive oxides is given in **Table 5**.

5. Applications of solution-processed functional oxides for TFTs and display

5.1. Low-temperature all solution-derived amorphous oxide TFTs

TFTs, in which all the layers were fabricated using simple chemical solution-processed, vacuum-free routes, followed by thermal annealing at 400°C, were demonstrated [34]. A ruthenium oxide (RuO_2) was used for both gate and source/drain electrodes. Amorphous LZO and zirconium-indium-zinc oxide (ZIZO) films were used as the gate insulator and channel layer, respectively, which enabled the fabrication of a TFT with the desired performance at a sufficiently low temperature. Transfer characteristics of the low-temperature all solution-processed TFT are shown in **Figure 10**. The obtained "on/off" ratio, *SS*-factor, and μ were ~6×10^5, 250 mV/decade, and 5.80 $cm^2 V^{-1} s^{-1}$, respectively.

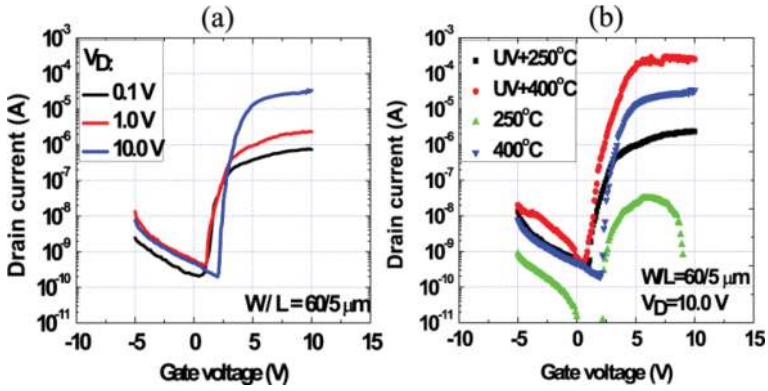

Figure 10. Transfer curves of low-temperature all solution-processed oxide TFT.

5.2. Electrophoretic display driven by all solution process active-matrix oxide TFTs

Precursor solutions and a solution process were developed for the fabrication of active-matrix amorphous oxide-TFTs [102]. The gate lines (GE), gate insulator (GI), and channel layer (CH) comprised RuO_2, LZO, and ZIZO films, respectively. The polysilazane-based silicon dioxide (PSZ) film was used for the channel stopper (CS) layer. The source and drain (S/D) electrode had a double-layer structure comprising ITO and RuO_2 films. The silsesquioxane-based silicon dioxide (SQ) and RuO_2 films were used for the passivation layer (PV) and pixel electrodes (PE), respectively (**Figure 11(a)**). Details of the precursor solutions and annealing conditions for the film formations are summarized in **Table 6**. The TFTs exhibited a μ of 2.68 $cm^2 V^{-1} s^{-1}$, a *SS*-factor of 1.09 V/decade, a V_{th} of 3.06 V, and an "on/off" ratio of 10^5. Electrophoretic displays (EPDs) with a resolution of 101.6 ppi were successfully fabricated using the all solution-processed active-matrix TFTs (**Figure 11(b** and **c)**). Bi-stable black/white images were retained after cutting of the power supply and video signal in these TFT-EPDs (**Figure 11(d)**). It is considered that low-cost electronic paper can be realized using this technology in the near future.

5.3. Direct printing of oxide TFT by nano-rheology printing

Among various solution-based approaches, a direct printing is a promising low-cost technique for fabricating oxide TFTs. The printing technique offers several advantages in manufacturing electronics such as a direct writing of materials, reduction of materials waste, and reproducibility with high resolution, which are not affordable from other solution-based approaches [103–105]. While many printed organic TFTs have been reported, relatively fewer studies, associated with directly printed oxide TFTs, have been pursued [17, 33, 106]. Furthermore, the printing has mainly been applied for metal-oxide semiconductor as the channel layer, while other layers such as GE, S/D, CS, and PV were fabricated by other techniques.

Recently, a new printing method, so-called nano-rheology printing (nRP), for metal oxide patterns within sub-micrometer range, was introduced [33]. The nRP method, which is a type of direct thermal imprinting, uses viscoelastic transformation like glass transition of oxide

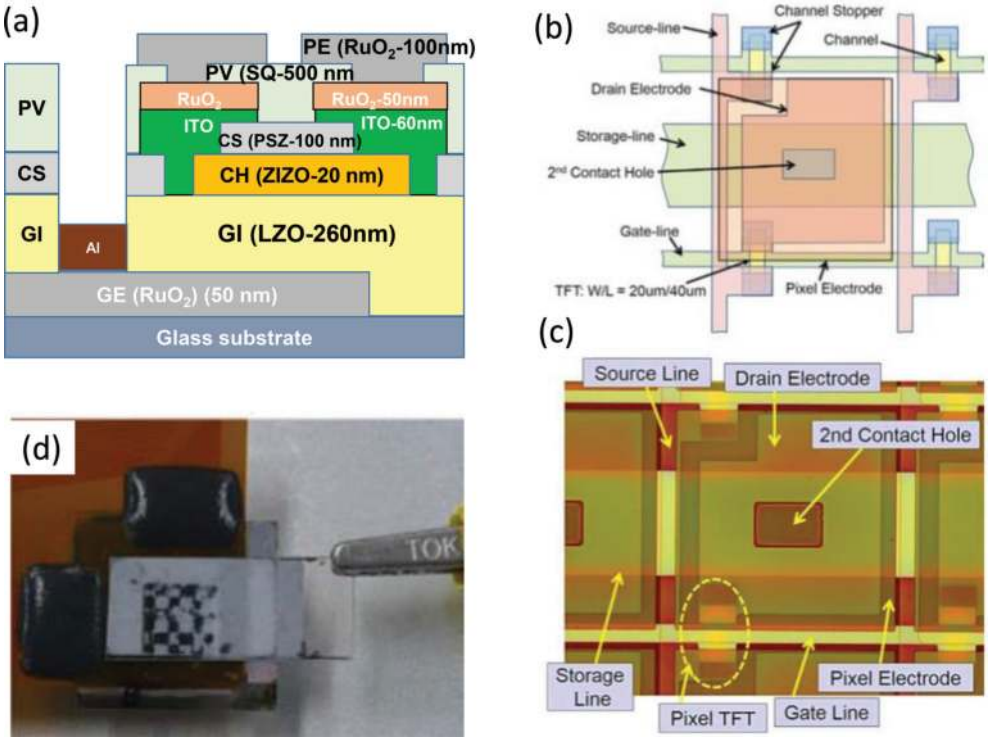

Figure 11. Cross-sectional structure of TFT (a), diagram of the pixel layout (b), and photograph of the pixels (c) in the TFT-driven electrophoretic display. The pixel pitch was 250 × 250 μm^2, which corresponds to a resolution of 101.6 ppi. The aperture ratio was 84.6%.

Layer	Materials	Precursor material	Solvent	Annealing condition
GE	RuO_2	$Ru(NO)(OAc)_3$	MEA, PrA	500°C/10 min
GI	LZO	$La(O_2C_2H_3)_3$, $Zr(OC_4H_9)_4$	PrA	550°C/O_2/10 min
CH	ZIZO	$Zr(OC_4H_9)_4$, $In(OCCH_3CHOCCH_3)_3$, $ZnCl_2$	PrA, 2ME	550°C/O_2/20 min
CS	SiO_2	Polysilazane		500°C/H_2O/30 min
S/D	RuO_2/ITO	$Ru(NO)(OAc)_3$, $In(NO_3)_3{\cdot}3H_2O$, acacH, NH_4Ac, $SnCl_2$	MEA, PrA, 2ME	500°C/air/10 min
PV	SiO_2	Silsesquioxane		500°C/O_2/10 min
PE	RuO_2	$Ru(NO)(OAc)_3$	MEA, PrA	250°C/air/5 min

MEA, 2-aminoethanol; PrA, propionic acid; 2ME, 2-methoxyethanol; acacH, acetylacetonate; NH_4Ac, ammonium acetate.

Table 6. The precursor solutions and annealing conditions for the film formations in all solution-processed TFT-FPD.

precursor gels when imprinted; it softens at a certain temperature during thermal imprinting so that the gel can be rheologically imprinted. The total process for the nRP method is illustrated in **Figure 12**. A thermal nanoimprinting machine (ST-50, Toshiba machine) has been

http://dx.doi.org/10.5772/intechopen.75610

used. First, a solution is coated and dried to make a semi-solid thin film (1). It is then loaded onto the heating stage of the imprinting machine, after which a mold is set onto the semi-solid film and pressure is applied (2). At this point, almost no deformation occurs. When the temperature is increased, the semi-solid film will suddenly soften at a certain temperature (2–3). The imprinting temperature (T_{im}) is maintained to complete the imprinting (3). Next, the temperature is lowered, and then, the mold is detached (4). Although a small amount of residual film is remained, it can be easily removed by etching in atmospheric air and other such simple methods. The etching process slightly reduces the sharpness of the edge but has no other significant influence on the pattern geometry. Well-defined patterns of various functional oxide materials including insulators (ZrO_2, SiO_2), semiconductors (IGZO, SnO_2), and conductors (La-Ru-O, ITO) with the size down to several 10 nm were successfully produced by the nRP method [33, 107]. The imprinted patterns show very small shrinkage during post annealing, thereby achieving a high-shape fidelity to the mold. This results from the metal-oxide condensation at imprinting. The viscoelastic transformation and metal-oxide condensation at imprinting constitute the basics for the nRP method, which is closely related to the cluster structure in the precursor gel. Operation of totally rheology-printed oxide TFT (nRP-TFT) has been demonstrated (**Figure 13**) [94]. The obtained "on/off" ratio, *SS*-factor, and μ were 10^7, 80 mV/decade, and 8.4 $cm^2\ V^{-1}\ s^{-1}$, respectively. Furthermore, excellent TFTs with sub-micron channel length could be completely printed by this method in an air ambient [33]. Active-matrix oxide-TFT array totally printed by the nRP method for display application has also been demonstrated [108], indicating great promise for large-area low-cost printed electronics application.

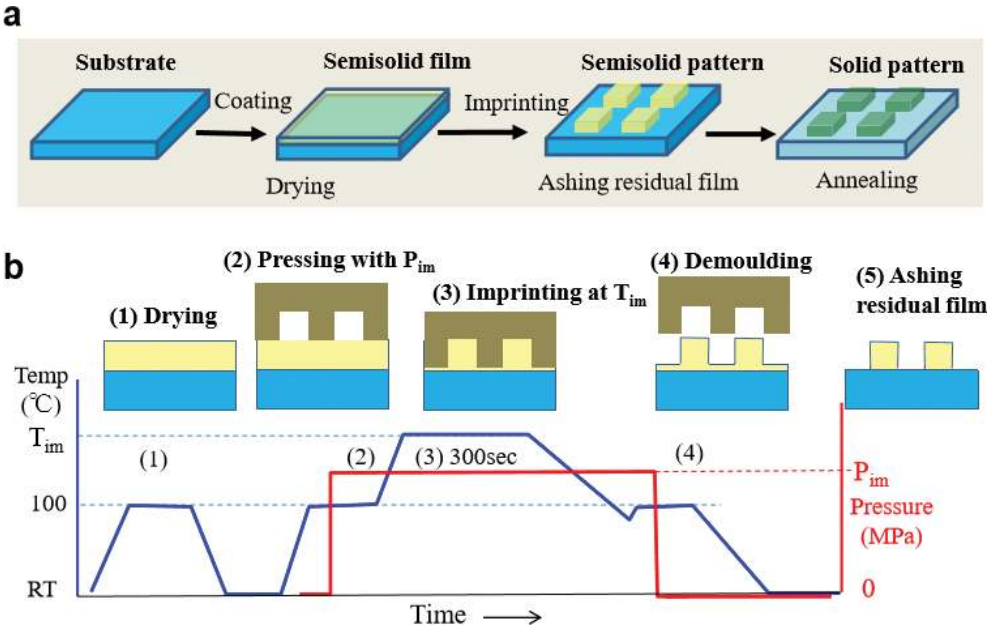

Figure 12. Process of the rheology printing. (a) Total process of rheology printing to form a one-layered pattern. (b) The profile of temperature and pressure during the imprinting process together with a schematic illustration of configurations of the imprinted film and the mold.

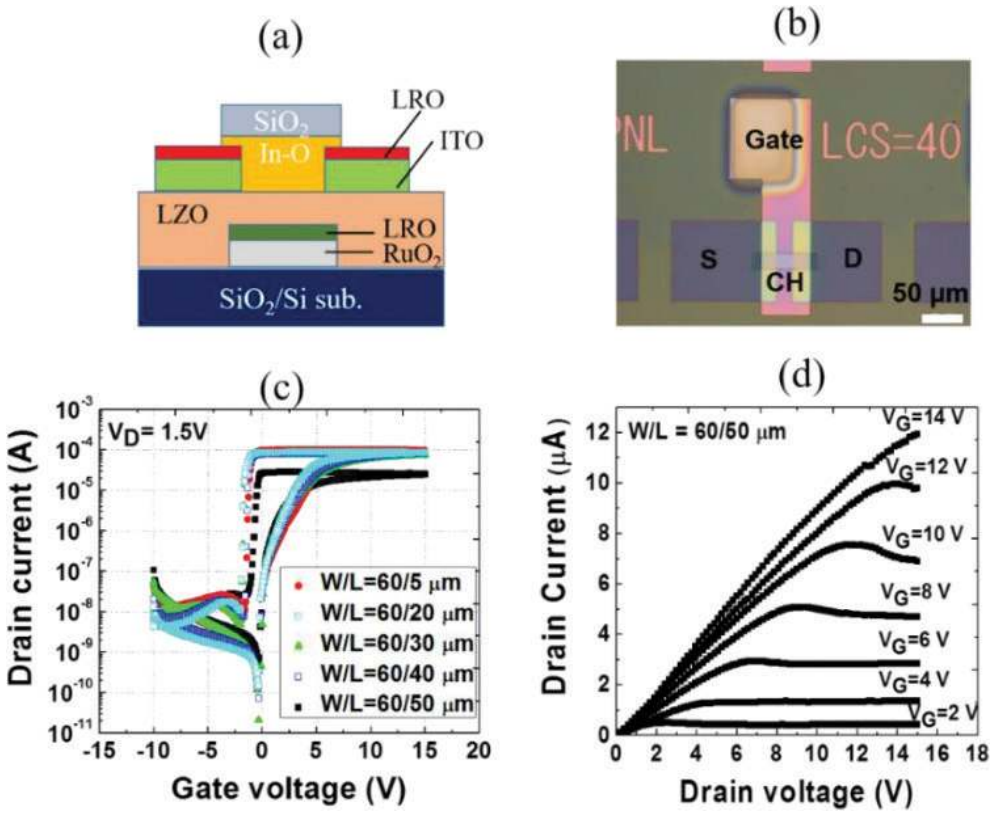

Figure 13. (a) Cross-sectional structure, (b) optical microscope image, (c) transfer curve, and (d) output curve of the nRP-TFT.

6. Conclusion

Solution-processed functional oxide materials deposited at a plastic-compatible temperature play a central role in the emerging printed electronic devices. The chapter critically reviews recent advances in the development of low-temperature solution-processable functional oxide materials including dielectric, semiconducting, and conductive thin-film oxides for printed electronics and highlights the challenges for the fundamental understanding and practical implementation of complex oxides in devices. Properties of oxide films and devices prepared from solution-based processes at a low temperature are now approaching those of vacuum-based counterparts. In addition, ultrahigh resolution printing technologies have been introduced enabling a feasible low-cost fabrication of electronic devices on a large area without the need of sophisticated lithography and vacuum systems. The remaining challenge lies in the production of p-type semiconducting oxide thin film whose performance must be improved to reach that of the n-type counterpart. Once both n-type and p-type oxide TFTs are ready, all-oxide CMOS, a building block of many electronic devices, can be realized.

Together with advanced printing technologies, it is expected that a truly printing of electronic devices has high potential to replace conventional production line in the near future.

Acknowledgements

The author thanks JST-ERATO Shimoda Nano-Liquid Process Project (2007–2014) and JST-CREST (2014–2019) for their financial supports. Special thanks go to members of Green Devices Research Center-JAIST and Center for Single Nano Innovative Devices-JAIST for their fruitful discussions.

Conflict of interest

The author declares that there is no conflict of interest.

Author details

Phan Trong Tue

Address all correspondence to: phan-tt@jaist.ac.jp

School of Materials Science, Japan Advanced Institute of Science and Technology, Nomi-shi, Ishikawa, Japan

References

[1] Yang JJ et al. Memristive switching mechanism for metal/oxide/metal nanodevices. Nature Nanotechnology. 2008;**3**:429

[2] Chen C-H, Suib SL. Control of catalytic activity via porosity, chemical composition, and morphology of nanostructured porous manganese oxide materials. Journal of the Chinese Chemical Society. 2012;**59**(4):465-472

[3] Gich M et al. Multiferroic iron oxide thin films at room temperature. Advanced Materials. 2014;**26**(27):4645-4652

[4] Vrejoiu I et al. Functional perovskites—From epitaxial films to nanostructured arrays. Advanced Functional Materials. 2008;**18**(24):3892-3906

[5] Hiroyuki A. Recent advances and future prospects in functional-oxide nanoelectronics: The emerging materials and novel functionalities that are accelerating semiconductor device research and development. Japanese Journal of Applied Physics. 2013;**52**(10R):100001

[6] Yu X, Marks TJ, Facchetti A. Metal oxides for optoelectronic applications. Nature Materials. 2016;**15**:383

[7] Glynn C, O'Dwyer C. Solution processable metal oxide thin film deposition and material growth for electronic and photonic devices. Advanced Materials Interfaces. 2017;**4**(2):1600610

[8] Nikam V, Bhuwalka KK, Kottantharayil A. Optimization of n-channel tunnel FET for the sub-22nm gate length regime. In: 2008 Device Research Conference. 2008

[9] Le Royer C. Interfaces and performance: What future for nanoscale Ge and SiGe based CMOS? Microelectronic Engineering. 2011;**88**(7):1541-1548

[10] Hu C. 3D FinFET and other sub-22nm transistors. In: 2012 19th IEEE International Symposium on the Physical and Failure Analysis of Integrated Circuits. 2012

[11] Hoffman RL, Norris BJ, Wager JF. ZnO-based transparent thin-film transistors. Applied Physics Letters. 2003;**82**(5):733-735

[12] Chiang HQ et al. High mobility transparent thin-film transistors with amorphous zinc tin oxide channel layer. Applied Physics Letters. 2005;**86**(1):013503

[13] Carcia PF, McLean RS, Reilly MH. High-performance ZnO thin-film transistors on gate dielectrics grown by atomic layer deposition. Applied Physics Letters. 2006;**88**(12):123509

[14] Yabuta H et al. High-mobility thin-film transistor with amorphous InGaZnO4 channel fabricated by room temperature rf-magnetron sputtering. Applied Physics Letters. 2006;**89**(11):112123

[15] Norris BJ et al. Spin-coated zinc oxide transparent transistors. Journal of Physics D: Applied Physics. 2003;**36**(20):L105

[16] David B, Mitzi MC, Murray CE, Kosbar L, Afzali A. Thin-film transistors based on spin-coated chalcogenide semiconductor channels. Proceedings-Electrochemical Society. 2005;**15**:10

[17] Lee DH et al. A general route to printable high-mobility transparent amorphous oxide semiconductors. Advanced Materials. 2007;**19**(6):843-847

[18] Srinivasan R et al. Crystallization and phase transformation process in zirconia: An in situ high-temperature X-ray diffraction study. Journal of the American Ceramic Society. 1992;**75**(5):1217-1222

[19] Ushakov SV, Brown CE, Navrotsky A. Effect of La and Y on crystallization temperatures of hafnia and zirconia. Journal of Materials Research. 2004;**19**(3):693-696

[20] John R. High dielectric constant gate oxides for metal oxide Si transistors. Reports on Progress in Physics. 2006;**69**(2):327

[21] Wilk GD, Wallace RM, Anthony JM. High-κ gate dielectrics: Current status and materials properties considerations. Journal of Applied Physics. 2001;**89**(10):5243-5275

[22] Wang L et al. High-performance transparent inorganic–organic hybrid thin-film n-type transistors. Nature Materials. 2006;**5**:893

[23] Ju S et al. Low operating voltage single ZnO nanowire field-effect transistors enabled by self-assembled organic gate nanodielectrics. Nano Letters. 2005;**5**(11):2281-2286

[24] Kukli K et al. Dielectric properties of zirconium oxide grown by atomic layer deposition from iodide precursor. Journal of the Electrochemical Society. 2001;**148**(12):F227-F232

[25] Park YM et al. Solution-processable zirconium oxide gate dielectrics for flexible organic field effect transistors operated at low voltages. Chemistry of Materials. 2013; **25**(13):2571-2579

[26] Yamada H et al. MOCVD of high-dielectric-constant lanthanum oxide thin films. Journal of the Electrochemical Society. 2003;**150**(8):G429-G435

[27] Yang C, Hang L, Xu J. Structural, optical and dielectric properties of HfSiO films prepared by co-evaporation method. Materials Science in Semiconductor Processing. 2015;**29**(Supplement C):321-325

[28] Talbot E et al. Atomic scale microstructures of high-k HfSiO thin films fabricated by magnetron sputtering. Materials Science and Engineering: B. 2012;**177**(10):717-720

[29] Yusuke O et al. HfO_2/Si and HfSiO/Si structures fabricated by oxidation of metal thin films. Japanese Journal of Applied Physics. 2009;**48**(5S1):05DA01

[30] Sokolov AS et al. Comparative study of Al_2O_3, HfO_2, and HfAlOx for improved self-compliance bipolar resistive switching. Journal of the American Ceramic Society. 2017;**100**(12):5638-5648

[31] Mikhelashvili V et al. Characteristics of metal-insulator-semiconductor capacitors based on high-k HfAlO dielectric films obtained by low-temperature electron-beam gun evaporation. Applied Physics Letters. 2004;**85**(24):5950-5952

[32] Li J et al. Hybrid cluster precursors of the LaZrO insulator for transistors: Properties of high-temperature-processed films and structures of solutions, gels, and solids. Scientific Reports. 2016;**6**:29682

[33] Kaneda T et al. Rheology printing for metal-oxide patterns and devices. Journal of Materials Chemistry C. 2014;**2**(1):40-49

[34] Tue PT et al. Low-temperature all-solution-derived amorphous oxide thin-film transistors. IEEE Electron Device Letters. 2013;**34**(12):1536-1538

[35] Tue PT et al. High-performance solution-processed ZrInZnO thin-film transistors. IEEE Transactions on Electron Devices. 2013;**60**(1):320-326

[36] Kim Y-H et al. Flexible metal-oxide devices made by room-temperature photochemical activation of sol–gel films. Nature. 2012;**489**:128

[37] Ridley BA, Nivi B, Jacobson JM. All-inorganic field effect transistors fabricated by printing. Science. 1999;**286**(5440):746-749

[38] Byrne PD, Facchetti A, Marks TJ. High-performance thin-film transistors from solution-processed cadmium selenide and a self-assembled multilayer gate dielectric. Advanced Materials. 2008;**20**(12):2319-2324

[39] Nomura K et al. Room-temperature fabrication of transparent flexible thin-film transistors using amorphous oxide semiconductors. Nature. 2004;**432**:488

[40] Mott NF. Silicon dioxide and the chalcogenide semiconductors; similarities and differences. Advances in Physics. 1977;**26**(4):363-391

[41] Narushima S et al. A p-type amorphous oxide semiconductor and room temperature fabrication of amorphous oxide p–n heterojunction diodes. Advanced Materials. 2003;**15**(17):1409-1413

[42] Hosono H. Ionic amorphous oxide semiconductors: Material design, carrier transport, and device application. Journal of Non-Crystalline Solids. 2006;**352**(9):851-858

[43] Kenji N et al. Amorphous oxide semiconductors for high-performance flexible thin-film transistors. Japanese Journal of Applied Physics. 2006;**45**(5S):4303

[44] Jeong S et al. Stable aqueous based cu nanoparticle ink for printing well-defined highly conductive features on a plastic substrate. Langmuir. 2011;**27**(6):3144-3149

[45] Jeong S et al. Printed Cu source/drain electrode capped by CuO hole injection layer for organic thin film transistors. Journal of Materials Chemistry. 2011;**21**(29):10619-10622

[46] Faber H et al. Low-temperature solution-processed memory transistors based on zinc oxide nanoparticles. Advanced Materials. 2009;**21**(30):3099-3104

[47] Schneider JJ et al. Synthesis, characterization, defect chemistry, and FET properties of microwave-derived nanoscaled zinc oxide. Chemistry of Materials. 2010;**22**(7):2203-2212

[48] Dasgupta S et al. Inkjet printed, high mobility inorganic-oxide field effect transistors processed at room temperature. ACS Nano. 2011;**5**(12):9628-9638

[49] Jeong S et al. Impact of metal salt precursor on low-temperature annealed solution-derived Ga-doped In_2O_3 semiconductor for thin-film transistors. The Journal of Physical Chemistry C. 2011;**115**(23):11773-11780

[50] Jeong WH, Bae JH, Kim HJ. High-performance oxide thin-film transistors using a volatile nitrate precursor for low-temperature solution process. IEEE Electron Device Letters. 2012;**33**(1):68-70

[51] Jeong S et al. Role of gallium doping in dramatically lowering amorphous-oxide processing temperatures for solution-derived indium zinc oxide thin-film transistors. Advanced Materials. 2010;**22**(12):1346-1350

[52] Banger KK et al. Low-temperature, high-performance solution-processed metal oxide thin-film transistors formed by a 'sol–gel on chip' process. Nature Materials. 2010;**10**:45

[53] Meyers ST et al. Aqueous inorganic inks for low-temperature fabrication of ZnO TFTs. Journal of the American Chemical Society. 2008;**130**(51):17603-17609

[54] Lin Y-H et al. High-performance ZnO transistors processed via an aqueous carbon-free metal oxide precursor route at temperatures between 80-180°C. Advanced Materials. 2013;**25**(31):4340-4346

[55] Kim M-G et al. Low-temperature fabrication of high-performance metal oxide thin-film electronics via combustion processing. Nature Materials. 2011;**10**:382

[56] Jun T et al. High-performance low-temperature solution-processable ZnO thin film transistors by microwave-assisted annealing. Journal of Materials Chemistry. 2011; **21**(4):1102-1108

[57] Carlos E et al. UV-mediated photochemical treatment for low-temperature oxide-based thin-film transistors. ACS Applied Materials & Interfaces. 2016;**8**(45):31100-31108

[58] Heo JS et al. Photochemically activated flexible metal-oxide transistors and circuits using low impurity aqueous system. IEEE Electron Device Letters. 2015;**36**(2):162-164

[59] Jaisutti R et al. Low-temperature photochemically activated amorphous indium-gallium-zinc oxide for highly stable room-temperature gas sensors. ACS Applied Materials & Interfaces. 2016;**8**(31):20192-20199

[60] Tsay C-Y, Liang S-C. Ultraviolet-assisted annealing for low-temperature solution-processed p-type gallium tin oxide (GTO) transparent semiconductor thin films. Materials Science in Semiconductor Processing. 2017;**71**:441-446

[61] Park SC et al. Advanced photo-annealing of indium zinc oxide films for thin-film transistors using pulse UV light. Journal of Information Display. 2016;**17**(1):1-7

[62] Rim YS et al. Simultaneous modification of pyrolysis and densification for low-temperature solution-processed flexible oxide thin-film transistors. Journal of Materials Chemistry. 2012;**22**(25):12491-12497

[63] Chen C et al. Solution-processed metal oxide arrays using femtosecond laser ablation and annealing for thin-film transistors. Journal of Materials Chemistry C. 2017;**5**(36):9273-9280

[64] Sun B, Sirringhaus H. Solution-processed zinc oxide field-effect transistors based on self-assembly of colloidal nanorods. Nano Letters. 2005;**5**(12):2408-2413

[65] Park SY et al. Low-temperature, solution-processed and alkali metal doped ZnO for high-performance thin-film transistors. Advanced Materials. 2012;**24**(6):834-838

[66] Han S-Y, Herman GS, Chang C-h. Low-temperature, high-performance, solution-processed indium oxide thin-film transistors. Journal of the American Chemical Society. 2011;**133**(14):5166-5169

[67] Oh H, Yang J-H, Hwang C-S. Ultralow-temperature sol-gel route to metal oxide semiconductors for soft platforms. Advanced Materials Interfaces. 2016;**3**(20):1600664

[68] Leppäniemi J et al. Rapid low-temperature processing of metal-oxide thin film transistors with combined far ultraviolet and thermal annealing. Applied Physics Letters. 2014;**105**(11):113514

[69] Minami T. New n-type transparent conducting oxides. MRS Bulletin. 2000;**25**(8):38-44

[70] Fraser DB, Cook HD. Highly conductive, transparent films of sputtered $In_{2-x}Sn_xO_{3-y}$. Journal of the Electrochemical Society. 1972;**119**(10):1368-1374

[71] Kim N-R et al. Enhanced conductivity of solution-processed indium tin oxide nanoparticle films by oxygen partial pressure controlled annealing. Journal of Materials Chemistry C. 2013;**1**(37):5953-5959

[72] Chen Z et al. Fabrication of highly transparent and conductive indium–tin oxide thin films with a high figure of merit via solution processing. Langmuir. 2013;**29**(45):13836-13842

[73] Kanehara M et al. Indium tin oxide nanoparticles with compositionally tunable surface plasmon resonance frequencies in the near-IR region. Journal of the American Chemical Society. 2009;**131**(49):17736-17737

[74] Lee J et al. A facile solution-phase approach to transparent and conducting ITO nanocrystal assemblies. Journal of the American Chemical Society. 2012;**134**(32):13410-13414

[75] Toki M, Aizawa M. Sol-gel formation of ITO thin film from a sol including ITO powder. Journal of Sol-Gel Science and Technology. 1997;**8**(1):717-720

[76] Ito T, Uchiyama H, Kozuka H. Evaporation-driven deposition of ITO thin films from aqueous solutions with low-speed dip-coating technique. Langmuir. 2017;**33**(21):5314-5320

[77] Tue PT et al. Combustion synthesized indium-tin-oxide (ITO) thin film for source/drain electrodes in all solution-processed oxide thin-film transistors. Applied Physics A. 2016;**122**(6):623

[78] Ban S-G et al. Low-temperature postfunctionalization of highly conductive oxide thin-films toward solution-based large-scale electronics. ACS Applied Materials & Interfaces. 2017;**9**(31):26191-26200

[79] Koo B-R, Bae J-W, Ahn H-J. Low-temperature conducting performance of transparent indium tin oxide/antimony tin oxide electrodes. Ceramics International. 2017; **43**(8):6124-6129

[80] Asakuma N et al. Low-temperature synthesis of ITO thin films using an ultraviolet laser for conductive coating on organic polymer substrates. Journal of Sol-Gel Science and Technology. 2003;**27**(1):91-95

[81] Ota R et al. Fabrication of indium-tin-oxide films by dip coating process using ethanol solution of chlorides and surfactants. Thin Solid Films. 2002;**411**(1):42-45

[82] Seki S et al. Highly conducting indium-tin-oxide transparent films prepared by dip-coating with an indium carboxylate salt. Surface and Coatings Technology. 2003; **169-170**:525-527

[83] Alam MJ, Cameron DC. Preparation and properties of transparent conductive aluminum-doped zinc oxide thin films by sol-gel process. Journal of Vacuum Science & Technology A: Vacuum, Surfaces, and Films. 2001;**19**(4):1642-1646

[84] Nanto H et al. Electrical and optical properties of zinc oxide thin films prepared by rf magnetron sputtering for transparent electrode applications. Journal of Applied Physics. 1984;**55**(4):1029-1034

[85] Fortunato E, Barquinha P, Martins R. Oxide semiconductor thin-film transistors: A review of recent advances. Advanced Materials. 2012;**24**(22):2945-2986

[86] Liu H et al. Transparent conducting oxides for electrode applications in light emitting and absorbing devices. Superlattices and Microstructures. 2010;**48**(5):458-484

[87] Beyer W, Hüpkes J, Stiebig H. Transparent conducting oxide films for thin film silicon photovoltaics. Thin Solid Films. 2007;**516**(2):147-154

[88] Kamiya T et al. Electrical properties and structure of p-type amorphous oxide semiconductor xZnO·Rh_2O_3. Advanced Functional Materials. 2005;**15**(6):968-974

[89] Kawazoe H et al. P-type electrical conduction in transparent thin films of $CuAlO_2$. Nature. 1997;**389**:939

[90] Kawazoe H et al. Transparent p-type conducting oxides: Design and fabrication of p-n heterojunctions. MRS Bulletin. 2000;**25**(8):28-36

[91] Kim S et al. Room temperature deposited oxide p-n junction using p-type zinc-cobalt-oxide. Journal of Applied Physics. 2010;**107**(10):103538

[92] Aksit M et al. Misfit layered $Ca_3Co_4O_9$ as a high figure of merit p-type transparent conducting oxide film through solution processing. Applied Physics Letters. 2014;**104**(16):161901

[93] Li J et al. P-type conductive amorphous oxides of transition metals from solution processing. Applied Physics Letters. 2012;**101**(5):052102

[94] Tue PT, Fukada K, Shimoda T. High-performance oxide thin film transistor fully fabricated by a direct rheology-imprinting. Applied Physics Letters. 2017;**111**(22):223504

[95] Li J et al. Highly conductive p-type amorphous oxides from low-temperature solution processing. Applied Physics Letters. 2012;**101**(13):132104

[96] Götzendörfer S, Bywalez R, Löbmann P. Preparation of p-type conducting transparent $CuCrO_2$ and $CuAl_{0.5}Cr_{0.5}O_2$ thin films by sol-gel processing. Journal of Sol-Gel Science and Technology. 2009;**52**(1):113-119

[97] Chen H-Y, Wu J-H. Transparent conductive $CuFeO_2$ thin films prepared by sol–gel processing. Applied Surface Science. 2012;**258**(11):4844-4847

[98] Chiu T-W et al. Preparation of p-type conductive transparent $CuCrO_2$:Mg thin films by chemical solution deposition with two-step annealing. Ceramics International. 2012;**38**:S673-S676

[99] Wang J et al. Combustion synthesis of p-type transparent conducting $CuCrO_{2+x}$ and Cu:CrO_x thin films at 180 °C. In: ACS Applied Materials & Interfaces. 2018

[100] Farrell L et al. Spray pyrolysis growth of a high figure of merit, nano-crystalline, p-type transparent conducting material at low temperature. Applied Physics Letters. 2015;**107**(3):031901

[101] Liu Y, Pollaor S, Wu Y. Electrohydrodynamic processing of p-type transparent conducting oxides. Journal of Nanomaterials. 2015;**2015**:14

[102] Inoue S et al. Electrophoretic displays driven by all-oxide thin-film transistor backplanes fabricated using a solution process. Physica Status Solidi (a). 2015;**212**(10):2133-2140

[103] Sirringhaus H et al. High-resolution inkjet printing of all-polymer transistor circuits. Science. 2000;**290**(5499):2123-2126

[104] Wang JZ et al. Dewetting of conducting polymer inkjet droplets on patterned surfaces. Nature Materials. 2004;**3**:171

[105] Shimoda T et al. Solution-processed silicon films and transistors. Nature. 2006;**440**:783

[106] Kim D et al. Inkjet-printed zinc tin oxide thin-film transistor. Langmuir. 2009;**25**(18): 11149-11154

[107] Nagahara K et al. Rheology printing of an ultra-fine conductive Ru–La–O line. Ceramics International. 2016;**42**(6):7730-7741

[108] Hirose D et al. All-solution-printed oxide thin-film transistors by direct thermal nano-imprinting for use in active-matrix arrays. Physica Status Solidi (a). 2017;**214**(1):1600397